Nonlinear ICRF-Plasma Interactions

J. R. Myra, D. A. D'Ippolito and D.A. Russell

Lodestar Research Corp., Boulder, Colorado 80301

L. A. Berry, E. F. Jaeger and M. D. Carter

Oak Ridge National Laboratory, Oak Ridge, Tennessee 37831

rev. Dec 2005

submitted to *Nuclear Fusion*

Nonlinear ICRF-plasma interactions

J. R. Myra, D. A. D'Ippolito, and D.A. Russell

Lodestar Research Corporation, Boulder, Colorado, USA

L. A. Berry, E. F. Jaeger, and M. D. Carter

Oak Ridge National Laboratory, Oak Ridge, Tennessee, USA

Nonlinear interactions of ion cyclotron range of frequency (ICRF) waves with fusion plasmas are reviewed. Although the linear theory of ICRF waves, including fast waves (FW), high-harmonic fast waves (HHFW) and ion Bernstein waves (IBW), is widely applicable, nonlinear effects can still be important, especially in the edge plasma, or for novel core applications. Here the topics of flow drive, ponderomotive forces, rf sheaths, parametric decay and related interactions with the edge plasma are considered. Primary emphasis is placed on basic underlying physics and tokamak applications. For FW antennas, the parallel electric field near launching structures is known to drive radiofrequency (rf) sheaths which can give rise to convective cells, interaction with plasma "blobs", impurity production, and edge power dissipation. In addition to sheaths, IBW waves in the edge plasma are subject to strong ponderomotive effects and parametric decay. In the core plasma, slow waves can sometimes induce nonlinear effects. Mechanisms by which these waves can influence the radial electric field and its shear are summarized, and related to the general (reactive-ponderomotive and dissipative) force on a plasma from rf waves. Standard ICRF codes have begun to incorporate the nonlinear topics described here. Further progress in integrated simulation should allow new predictive modeling capabilities.

PACS: 52.40.Kh, 52.35.Mw, 52.40.Fd

1. Introduction

Ion cyclotron range of frequencies (ICRF) waves have been routinely used in magnetic confinement experiments for heating plasmas and driving currents. The most commonly employed waves today are the fast wave (FW), including the high-harmonic fast wave (HHFW), and ion Bernstein wave (IBW). The linear theory of these waves is both widely applicable to experiment and exceedingly rich in the complexity and subtlety of physical phenomena which it can describe. This fact underlies many decades of successful theoretical research in ICRF wave physics.

In spite of this, there are important situations in which linear physics fails, and nonlinear effects can become important. The nonlinear effects of interest fall broadly into two categories: surface effects such as rf sheaths which are governed by rf voltages (V_{rf}) and volume effects such as ponderomotive interaction and nonlinear wave coupling which are governed by the "jitter" velocity u_{rf}, and/or its close relatives, the species ponderomotive potential (jitter energy) $\Psi \sim \frac{1}{2} m u_{rf}^2$ and the wave energy density (W_{rf} typically of order $n\psi$, for electrostatic waves in a plasma), where m is the particle mass and n is the plasma density. Although many important details influence the onset of "significant" nonlinear interaction in specific applications, one would *a priori* expect nonlinear effects to be important when $eV_{rf} \sim T$, $\Psi \sim T$ and $W_{rf} \sim nT$ respectively, where T is the plasma temperature. More refined estimates of these criteria will be presented in the appropriate sections to follow.

The most obvious case in which to consider nonlinear effects is near the antenna where the rf fields are large, and typical rf voltages and/or ponderomotive potentials

easily exceed T/e. Wave-induced rf sheath voltages can also exceed T/e near walls and limiters where the plasma temperature is low. Additionally, slow waves, which have a small group velocity and therefore require a large electric field (i.e. a large W_{rf}) to carry power are particularly susceptible to nonlinear effects. Significant wave energy density relative to the plasma thermal energy can be expected to trigger parametric decay and/or nonlinear wave-wave self-interaction in the edge plasma. Nonlinear effects due to slow waves can also sometimes be important in the core plasma where the interactions can drive plasma flows and radial electric field shear, of interest for turbulence suppression and transport barrier formation. When flow damping by neoclassical or other processes is weak, flows of interest may be sought in situations for which W_{rf}/nT is small.

The goal of this paper is to summarize physics concepts in these areas where nonlinear effects enter, indicate available modeling and analysis tools, and point out opportunities for new predictive capabilities. Although experimental motivation will be given, this paper will not attempt a comprehensive experimental review. Many of the relevant older experimental references have been given elsewhere [1-3] and will not be repeated here, but some newer experimental work will be described. Special emphasis in this mini-review will be given to topics of contemporary interest for the ICRF modeling community, and a few new recent results will be presented. Our paper extends a recent conference proceedings paper [4] on the same subject.

To place the material which follows in better context, we consider briefly the pertinent properties of the various types of rf waves which enter the discussion. The FW and HHFW are on the fast compressional Alfvén wave branch. These waves, which have phase (and group) velocities on the order of the Alfvén velocity, are elliptically,

approximately right-hand polarized, waves with the rf electric field $\mathbf{E} \approx \mathbf{E}_\perp$ almost normal to the equilibrium magnetic field. The plasma response to the pure FW tends to be linear under conditions normally prevalent in the core of fusion heating and current drive experiments (somewhat less so in the edge). However, and more importantly as we shall see, nominal "FW" launching structures do not couple exclusively to the FW branch, and interactions of the FW with the edge boundaries as well as interior mode-conversion layers can cause the FW to generate other waves with inherently more nonlinear properties.

In addition to the FW, the IBW has been employed for plasma heating, flow drive and other applications in many fusion experiments. [3] The IBW is approximately an electrostatic, short wavelength mode with wavelength on the order of the ion Larmor radius and frequencies between, and often near, the harmonics of the cyclotron frequency. The polarization of the rf electric field of the IBW is also dominantly perpendicular to the equilibrium magnetic field. Because the group velocity of the IBW is typically small (on the order ion thermal velocity) the IBW is an example of a wave that can be highly nonlinear, with large electric field, even at modest power levels.

In experiments, the IBW is sometimes launched into the plasma through the process of mode transformation from its low density, cold fluid counterpart, the electron plasma wave (EPW). [3] Thus, to understand the behavior of nominal "IBW" launching structures, one must consider the properties of the EPW. At ion cyclotron frequencies, which are typically much less than the electron plasma frequency, the EPW propagates almost normal to the magnetic field, B_0, provided that the density is low (less than the lower-hybrid density), and the large electron plasma response parallel to B_0 is reduced by

the small projection angle. In the electrostatic limit, this mode has a projection of the rf electric field onto $E_\parallel$ and this can give rise to ponderomotive forces which can often be quite strong.

Finally, as mentioned above, the FW can convert to short wavelength modes at mode-conversion layers, such as the IBW and the ion-cyclotron slow wave (ICW). These conversions tend to be favored in multi-component plasmas when the minority density is large. The ICW is on the slow torsional shear Alfvén wave branch, is approximately left-hand polarized and propagates below the ion cyclotron frequency in a single-ion-species plasma. It was directly employed for "magnetic beach heating" in early, low density, fusion experiments. Because it is a slow wave, the ICW is susceptible, especially near cyclotron resonance, to nonlinear effects. It will be of particular interest in a mode-conversion, flow-drive application to be considered in Sec. 4.

The outline of our paper is as follows. In the next section we consider edge interactions from rf sheaths arising in experiments which launch the fast wave (FW). This section includes a discussion of basic sheath physics, antenna (near-field) sheaths and far-field sheaths. This is followed by a discussion of additional effects present in ion Bernstein wave (IBW) direct launch experiments. Then IBW and ion cyclotron wave (ICW) core interactions and driven flows are reviewed. The final section presents some thoughts on the opportunities and prospects for future theoretical work involving integrated computer modeling.

Several nonlinear topics are outside the scope of this paper. In the antenna region, we do not consider the highly nonlinear physics of rf-driven arcs, breakdown, and out-gassing, although these subjects are certainly of great practical importance for ICRF

antennas in fusion experiments. In the core, we omit consideration of 2nd-order nonlinear physics of quasilinear diffusion and Fokker Planck interactions, and the subsequent evolution of particle distributions. This topic is discussed elsewhere in the present issue. [5] Also omitted are the nonlinear interactions that occur on the transport time scale when nonlinear rf waves heat, and drive currents, modifying the equilibrium and its MHD stability properties.

2. FW edge interactions: rf sheaths

In this section we consider nonlinear interactions in the context of experiments that nominally launch the fast wave. Importantly, typical antenna launching structures will be seen to couple significantly to $E_{||}$ (i.e. the slow wave), and this coupling is argued to be the root cause of the nonlinear interactions seen in a wide class of experiments.

It is also significant that the FW is usually evanescent at the low-density plasma edge, owing to the right-hand cut-off. [6] As a consequence, good coupling of the antenna to the plasma requires that the antenna be placed close to the plasma, and this in turn opens up the possibility of nonlinear plasma interactions. Furthermore, because antenna coupling is heuristically proportional to local density, and the plasma density can be governed by local nonlinear rf physics, the edge plasma - antenna system can behave as a strongly nonlinear coupled system.

A variety of rf edge interactions have been seen on ICRF experiments for several decades, as reviewed in [1, 2]. For example, a particularly systematic study was carried out on JET, which serves to illustrate the scope of the problem. The observed rf specific effects included: impurities (due to RF-enhanced sputtering) [7,8], uncontrolled

instantaneous density rise [9], arcs [8], antenna damage, and anomalous edge power dissipation [8]. The rf antenna voltage controls these near-field rf-specific effects, which are generally least severe in anti-symmetric (e.g. dipole) phasing. [7,8] Experience and intuition developed over the years have led to the mitigation of deleterious effects in most dipole heating experiments. But, it is likely that rf-edge interactions will have important implications for present and future experiments requiring FW current drive and long pulse operation, where even small effects can have large consequences.

A. Basic sheath physics

The primary culprit for many of the observed phenomena is the rf sheath which exists at "end-plates" where the field line contacts a conductor. Important places where rf sheaths occur will be identified later. The basic physics underlying a sheath is illustrated in Fig. 1. Both species, electrons and ions, initially try to leave at their respective thermal velocities. In response to the growing charge imbalance, the plasma develops a potential to confine the electrons and restore charge ambipolarity. This potential, which must be higher than the applied voltage at either of the two ends, reflects almost all of the electrons at the sheath entrance. The sheath width $\Delta \sim \lambda_d (eV/T_e)^{3/4}$ at each end is determined by requiring that the un-neutralized ion space charge in the sheath layer is sufficient to give rise to the required potential drop. Here λ_d is the Debye length, e the proton charge, V the applied voltage and T_e the electron temperature. In addition to reflecting electrons, this large sheath accelerates ions into the plates, creating a fast ion distribution which enhances physical sputtering. The energy for this acceleration comes from the circuit, and appears as lost power to the sheath. The whole process is driven by the need for charge ambipolarity.

This basic sheath physics extends immediately into an ICRF sheath, [10-15] where an oscillating voltage is applied to each plate. Electrons leave alternately out one end, then the other, escaping from the end where applied voltage is highest (and hence the reflecting barrier seen by the electrons lowest). This give rise to an oscillating parallel electron current. The central voltage oscillates up and down at twice the applied frequency, but always remains higher than the applied voltage at either end. The net effect is that there is both rectification of the applied voltage and a large second harmonic. The net sheath power dissipation (for the case of Maxwell-Boltzmann electrons) is given by [16, 17]

$$P_{sh} = n_e c_s A T_e \xi I_1(\xi) / I_0(\xi) \rightarrow n_e c_s A e V_{rf} \qquad (1)$$

where $n_e c_s$ is the plasma flux, A is the projected area normal to the magnetic field, $\xi = eV_{rf}/T_e$, I_0 and I_1 are Bessel functions, and the final form is the high voltage limit. The two most important parameters are the plasma density (and flux) into the antenna, and the rf voltage.

Several other considerations are important, including the angle at which the field line strikes the plate, and the fast ion energy distribution. The field line angle influences the ion orbits in the sheath, and impacts surface physics calculations such as sputtering. Simulations have been performed to quantify these and other effects. [11-13] In particular, for shallow incidence of the field lines onto the surface, there is a significant magnetic presheath in which the ion flow transitions from being sonic along the field lines to sonic normal to the plate. [13] These types of calculations confirm that the sheath voltage drop available for ion acceleration and power dissipation is normally an order unity fraction of the applied rf voltage (i.e. fast ion energy ~ ZeV_{rf}), because the

potential drop in the sheaths is largely controlled by electron physics and simple ambipolarity considerations.

It should be clear from this discussion that rf sheath effects dominate thermal (Debye) sheaths locally whenever $eV_{rf}/T_e > 1$. The rf sheaths in the vicinity of an antenna (see section B, following) easily satisfy this condition, having V_{rf} of typically hundreds of volts, and reaching kilovolts or more in extreme cases. Thus, the ion impact energy onto the surface is of order ZeV_{rf}. However, the net significance of rf sheaths in experiments depends on the local plasma density, the total affected area of the tokamak, and other factors such as material surface properties.

One of the goals that is being pursued in contemporary research is that of including plasma and rf-sheath effects in antenna coupling codes. Since it is still impractical to do full wave particle simulations for the rf fields and sheaths, it is important to be able to characterize the main effect of the sheaths in a simple way. A useful model [18] is to regard the electrons as an oscillating charge layer, which leaves a vacuum gap in the rf sheath. As far as the rf is concerned, this vacuum gap provides an extra capacitance in the rf circuit. This type of model was investigated [19] for plasma processing and is currently being tested in an rf antenna coupling code for fusion applications. [20] The presence of rf sheaths can modify the rf-field distribution between antenna bumper limiters.

Utilizing the fact that the sheath is a thin layer, it is also possible to analytically derive a "sheath boundary condition" that can replace the usual perfect conductor boundary conditions $\mathbf{E}_t = B_n = 0$ on the surface of a conductor where $\mathbf{E}_t$ is the tangential component of $\mathbf{E}$ and B_n the normal component of $\mathbf{B}$. [21, 22] The resulting sheath

boundary condition shows that $\mathbf{E}_t \sim (\Delta/\varepsilon_{sh}) \nabla_t D_n$ where $\mathbf{D} = \boldsymbol{\varepsilon} \cdot \mathbf{E}$ is computed on the plasma (computational domain) side of the sheath with dielectric tensor $\boldsymbol{\varepsilon}$, ∇_t is the tangential projection of the gradient, D_n is the component of $\mathbf{D}$ normal to the sheath, Δ is the sheath width and $\varepsilon_{sh} \sim 1$ (for a near vacuum sheath) is the effective dielectric in the sheath layer, which can model both sheath capacitance and dissipation (resistance). This formulation is equivalent to the vacuum gap model, where the sheath enters as a volumetric circuit element. [19] Because the sheath power dissipation and sheath width depend nonlinearly on the sheath voltage (given from the model in terms of the surface electric fields) implementation of this boundary condition in an rf-wave code would require iteration for a self-consistent result. It offers the hope of a relatively simple model in which some nonlinear sheath effects can be incorporated into existing codes, allowing self-consistent simulation of sheath power dissipation and the effect of the sheaths on the rf field pattern in realistic geometries.

An interesting and important question concerning self-consistent rf coupling codes and sheath interactions is the competition associated with the plasma density near the antenna. A large density is favorable for good coupling (because the launched FW is usually evanescent at low densities) but this also increases the level of sheath interaction. These considerations are partly addressable in antenna design, for example by using septa and bumper limiters. [7, 23]

B. Antenna (near-field) sheaths and interaction with edge plasma

RF sheaths occur where field lines containing plasma contact conducting surfaces. On the antenna itself, the geometry of these connections implies a phasing and field line angle dependence [24], as illustrated in Fig. 2. For a two-strap antenna in $0\text{-}\pi$ (dipole)

phasing, and symmetrical sheath connections on the front face of the Faraday screen, there is no net rf voltage induced between contact points. This point can be verified by considering the induction circuit, i.e. the net rf-magnetic flux that crosses the field line illustrated in Fig. 2, taking the symmetry into account. In dipole phasing the net flux is zero. However in 0-0 (monopole) phasing a net flux and hence a large voltage can result. The voltage in this case is essentially the fraction of the end-to-end voltage along the current strap that is subtended by the contacts.

This kind of Faraday screen rf sheath is exacerbated by large misalignment of the equilibrium B-field with the Faraday Screen and/or a large component of B along the current strap, and by low-$k_{\parallel}$ non-symmetric phasings. (A useful analytic model of these dependences is given in Eq. (5) of [16].) As a result, experiments have shown that ICRF heating in dipole phasing is much easier than ICRF current drive, which requires low-$k_{\parallel}$ phasings. It is possible, in theory, to construct *multiple-strap* current drive antennas which cancel induced voltages on the long field line connections [16, 25], however, other considerations are also relevant, as discussed next.

The simple inductive picture of sheaths presented in Fig. 2 is complicated in practice by geometrical effects and the finite phase velocity of electromagnetic waves flowing through the coupled antenna-plasma system. Corner effects drive rf sheaths [25, 26] because field lines that cut across the corner of the antenna do not see anti-symmetric, canceling rf magnetic fluxes in 0-π phasing. Thus, while the induced sheath voltages in 0-π phasing are smaller than in 0-0 phasing, they are not zero in the corners. In addition, rf charges can appear throughout the antenna structure because of the finite phase velocity of waves traveling over conductors and in the plasma near the antenna.   These

displacement current effects lead to $\nabla\cdot\mathbf{J} = -\partial\rho/\partial t \neq 0$, and are further complicated by an asymmetric plasma response [27]. The electric fields associated with charges from any of these effects can drive rf sheaths.

In general, quantitative sheath analysis for antennas can only be done with the aid of 3D rf antenna codes that can take into account the complicated electric field structure and antenna structure. At present, while a number of such codes exist, they all assume a vacuum in the antenna region itself. This forecloses for the moment the interesting possibility of direct simulation in these 3D codes of self-consistent plasma-antenna interaction due to rf-sheaths. However, 3D antenna codes have been used to "calibrate"' 2D antenna codes in which the rf-sheath plasma-antenna interaction can be studied. [20] Particle in cell (PIC) methods may eventually allow direct simulations of 3D sheath-plasma-antenna interaction.

Due to the grazing nature of the field lines contacting the complicated three-dimensional structure of an antenna, the contact points are very sensitive to field line location, and adjacent field lines can end up having very different induced sheath voltages because their induction circuits trap a different amount of rf magnetic flux. This is illustrated in Fig. 3 using the results of a vacuum antenna code to model the 3D antenna structure and rf fields for a mock-up of a TFTR FW antenna, operated in 0-0 phasing [26]. When adjacent field lines charge to different voltages, there is a perpendicular electric field between them. This gives rise to $\mathbf{E}\times\mathbf{B}$ drifts and the important concept of rf-sheath-induced convection. [28-30]

The effects of rf-induced convection have been seen indirectly in experiments. On JET, reduced particle confinement and increased scrape-off-layer (SOL) density scale

length during monopole H-modes were attributed to rf-induced convection. [28] In Tore Supra the up/down heat flux asymmetry on the antenna was interpreted as arising from a large-scale rf-sheath driven convection roll pattern in front of the antenna. [31-34] This convection occurs because the antenna acts like a giant biased probe, charging positive all the field lines in front of it. The tokamak magnetic field gives a preferred direction to the $\mathbf{E} \times \mathbf{B}$ drift pattern and is responsible for convecting plasma preferentially into the bottom (or top) of the antenna (depending on the direction of B). Advances in edge plasma diagnostics, such as infrared (IR) imaging have allowed direct observation of rf-sheath-induced "hot spots" as illustrated in Fig. 4. Recently, [32] it has been demonstrated that this heat flux asymmetry reverses with reversal of the tokamak B-field, consistent with the rf-driven convection mechanism (although power flow asymmetries due to the Hall term may also play a role [35]).

Rf convection increases the flux of plasma into the antenna, thereby increasing the strength of rf-sheath interactions such as sputtering, sheath ion acceleration, and electron heating from interaction with the oscillating sheaths [36]. Importantly, it also modifies the electron density profile in front of the antenna. Reflectometers were used to measure this effect on TFTR and show that the antenna effectively pumps on the edge plasma (see Fig. 5) in agreement with theoretical models [37].

Thus, the rf antennas modify the edge density profile which in turn controls the antenna coupling. To treat this interaction theoretically, we consider the time-averaged vorticity or charge-balance equation,

$$\frac{c^2}{4\pi v_a^2} \frac{d}{dt} \nabla_\perp^2 \Phi = \nabla_\parallel J_\parallel + \frac{2c}{B} \mathbf{b} \times \kappa \cdot \nabla p \qquad (2)$$

where v_a is the Alfvén velocity and κ is the curvature. The currents which contribute to the dynamics in Eq. (2) are ion polarization currents across the magnetic field, parallel currents which terminate on sheaths, and magnetic field line curvature. The perpendicular polarization current, which appears as the charge advection term on the left of Eq. (2), couples flux tubes in the perpendicular direction. The parallel current term describes the 1-D sheath dynamics along the field line that was considered earlier. The curvature term, usually neglected in rf physics, gives rise to low frequency edge turbulence. The edge instabilities driven by this term eject filaments of plasma called blobs into the scrape-off-layer (SOL). These blobs convect towards the antenna by a simple mechanism. [38, 39] Curvature drift creates a charge separation. This gives rise to an internal electric field inside the plasma blob. The blob then convects radially as a whole due to the **E**×**B** drift. Consequently, the subject of antenna-plasma interaction is entwined with that of blobs and edge turbulence, and this interaction is fundamental to calculating the self-consistent SOL density profile in front of the antenna. [22] This *self-consistent* density is required for studies of rf coupling, impurities, antenna damage and other antenna interaction effects.

The interaction of blobs generated by edge turbulence with antenna near field sheaths has been studied using the 2D nonlinear fluid turbulence code, SOLT. [40] The model solves Eq. (2) coupled to a continuity equation. The nonlinear rf physics enters through the $J_{\parallel}$ term which includes the time-averaged (over the rf cycle) currents in the presence of sheath physics, using a Bessel model similar to that employed in Eq. (1). The interaction of the blob with the rf-sheath fields is strongly nonlinear, because the rf sheath voltage greatly exceeds the plasma temperature and typical edge turbulence-generated

potentials. The 2D simulations show that the interaction of rf waves with SOL turbulence is a rich and interesting subject, which also has important practical consequences. Results are shown in Fig. 6 for the case $eV_{rf}/T_e = 4$. The blob propagates into the antenna, where it is strongly sheared by the rf sheath fields, and then decays. Thus, the self-consistent density profile near the antenna arises from a superposition of turbulence-generated blobs, modified by antenna-sheath-driven convection, together with ionization of local neutrals (not included in this model).

Although the total power going into rf sheaths is most problematic at high power, at low power this same effect can be beneficially used to diagnose rf sheaths [16]. Since the sheath power dissipation P_{sh} is linear with the voltage for $eV/T_e > 1$ [see Eq. (1)], its contribution to the loading resistance $R_L = \frac{1}{2} P (Z/V)^2$ in this low (but not too low) power regime scales like $1/V$ and is larger than the loading due to the fast wave with $P_{FW} \propto V^2$. [At *very* low powers, where $eV/T_e << 1$, Eq. (1) again predicts $P_{sh} \propto V^2$; however, this limit is not of much practical interest for antenna sheaths.] Thus, sheath power can dominate the loading – a useful result for diagnosing the existence and properties (area, local density and voltage) of rf sheaths experimentally, and potentially useful for validation of antenna-sheath codes. This effect, illustrated in Fig. 7, has been observed [41] and successfully modeled [16] to show that sheath area, voltage and ambient density (or particle flux to the antenna) are the most important parameters. Again, it should be emphasized that while the fractional power lost to near-field antenna sheaths is always small for sufficiently large sheath (antenna) voltages, in the high power regime even a small fractional power loss can be quite damaging, if that power is deposited in a small volume for a long time. Thus diagnosis of sheaths in the low power loading regime for

the purpose of high power amelioration is a potentially important strategy for future long pulse machines.

The ubiquity of antenna sheaths has motivated work into sheath mitigation by the use of insulating materials. [42] On Phaedrus it was shown that the plasma potential rise due to rf sheath rectification could be almost completely eliminated by employing insulating limiters to intercept the field lines before they contact the metal, and complete the sheath circuit. [43] Effectively, the insulator adds an additional series impedance to the plasma sheath and absorbs most of the voltage drop that would otherwise appear across the sheaths. The main challenge with this strategy is to come up with insulating materials that can withstand a reactor environment. Boron compounds are often used in present day experiments, but novel ceramic materials have also been investigated. [44, 45]

When field lines are sufficiently long (so that the plasma resistance supports a significant voltage drop along the field line) the sheaths at the two ends become "disconnected". When these sheaths are also asymmetric (different voltages), they can drive a net dc parallel current. This effect was studied on TEXTOR, [46] and more recently on JET [47] where it was found that the sheath driven currents can trigger arcs at the high voltage end in some situations. This occurred in mixed phasing experiments where there was a current path between powered monopole and dipole antennas. In this case the cross-field polarization current driven by rf convection was postulated to be part of the current path, i.e. there was no direct field line connection between the antennas.

In addition to the various rf-specific sheath-related effects considered so far, there are other classes of nonlinear edge plasma effects that enter rf experiments. A particularly

notable one is the sputtering interaction of ions accelerated by the rf sheaths into the material surface of the antenna. The sputtering coefficient (the number of neutral surface atoms released by an incident ion) is a sensitive function of incident ion energy, angle, and target material and can exceed unity. [48] Sputtered neutrals are ionized in the edge plasma, and a certain fraction of these ions can be accelerated through the sheath to the surface, creating the possibility of an unstable feedback loop, or sputtering avalanche [24]. Sputtering exemplifies a class of plasma-surface interactions which, while not rf-specific, is exacerbated by the presence of rf wave energy (in this case the strong rf sheaths). Many other complex plasma-surface interactions (e.g. outgassing and local ionization, secondary electron emission and arcing) could be similarly modified and remain to be studied in detail.

In summary, past work has identified many of the key physics ingredients related to "near-field" or antenna sheaths and translated these into requirements of good antenna design. These include the use of good antenna-B field alignment, anti-symmetric (dipole) phasing, and insulating limiter coatings to minimize sheath voltages, use of antenna protection limiters to reduce the density (and particle flux) at the antenna, and use of appropriate antenna materials to reduce sputtering (and self-sputtering) coefficients. In regard to antenna materials, a dramatic illustration of this effect was given by the early JET experiments [7,8] contrasting the properties of Ni and Be Faraday screens and by the supporting modeling of impurity fluxes [24] showing the advantages of using low-Z materials. While it is possible to design a two-strap ICRF antenna with dipole phasing to heat the plasma with minimal sheath interactions, the multiple-strap antennas intended for heating and current drive on long-pulse machines require difficult compromises. Future

progress in this area will require 3D rf antenna codes with sheath boundary conditions for accurate modeling, new antenna and limiter materials, and new diagnostic techniques, such as low-power sheath loading. Some progress on the important problem of the self-consistent interaction of edge turbulence with antenna near-fields has been reported here, and more work in this area is required.

C. Far-field sheaths

So far the discussion has been confined to sheath losses local to the antennas, i.e. *near-field* sheaths. But edge parasitic power losses are often observed in low single-pass and low-$k_{\parallel}$ phasing situations where near field sheaths do not appear to explain the whole story. One concept which can relate very well to this type of observation is that of the *far-field* sheath, which gives a general mechanism for dissipation of wave energy in the SOL.

Edge rf fields appear on walls and limiters due to poor single pass absorption, or direct coupling to edge and surface modes. [12] Because the flux surfaces are not generally aligned with conducting boundaries, the FW polarization alone cannot satisfy the proper boundary conditions, and of necessity a slow wave with $E_{\parallel}$ is generated. [49, 50] This slow wave is often evanescent. This mechanism is illustrated by model calculations [50] shown in Fig. 8. The presence of an $E_{\parallel}$ in the boundary plasma brings into play all of the sheath effects that have been discussed so far in the near field antenna context. In particular, far field sheaths give a mechanism for edge power loss and impurity generation. Other dissipation mechanisms for waves at the edge are also possible, for example collisional dissipation of wave energy [12] by neutral collisions. The low-$k_{\parallel}$ modes, being less evanescent in their propagation from the core towards the walls, are most susceptible to these dissipation mechanisms. In this respect, the

evanescent region at the plasma edge is a "two-edged sword": it is detrimental to good antenna loading, but it is beneficial in reducing rf fields near walls and limiters by isolating core propagating modes from them.

Finally, a related but distinct parasitic loss mechanism occurs when the antenna couples to weakly damped eigenmodes. In this case, both near-field and far-field absorption are possible. Far-field absorption on the walls will depend on edge-core coupling as discussed above. The near-field antenna sheaths can be important because the antenna voltage is enhanced by nearly resonant global eigenmodes. [51, 52] A full analysis of these situations will require the integration of sheath physics and antenna coupling into full wave global codes.

3. IBW edge interactions: ponderomotive effects, parametric decay

In this section we turn our attention from FW experiments to IBW experiments. It is important to emphasize at the beginning that sheaths can be just as important for IBW edge interactions as in the FW case of the preceding section, and a direct application of these concepts may be made. [53] However, the IBW case also allows a rich variety of other nonlinear physics, primarily because Bernstein waves have a small group velocity and consequently require large electric fields to carry a significant power flux. Thus we will concentrate here on other nonlinear interactions: primarily ponderomotive effects, and parametric decay. This section considers mostly nominal IBW launch experiments; however, in some cases, the launcher may in fact couple to the closely related EPW. In more extreme cases, the underlying nonlinear mechanisms may also be relevant to FW experiments, as will be noted.

The linear theory of IBW coupling is rather well developed and has been reviewed by Ono [3] where interesting experimental results and nonlinear mechanisms are also reported. IBW coupling has met with mixed success and linear theory alone fails to describe many experiments. Coupling of power to the core has generally been better on small machines, and IBW experiments benefit from good conditioning. In a number of cases, the application of IBW power has failed to heat the core plasma at all. Here we review some nonlinear effects which bear on the issue of getting IBW power through the SOL into the core, noting that in some cases the same physics can also be relevant to nominal FW and high harmonic fast wave (HHFW) experiments where the large pitch of B relative to the antenna current strap results in substantial $E_\parallel$ (slow wave) coupling.

Ponderomotive expulsion of plasma is one of the expected nonlinear mechanisms. For the slow wave, the (repulsive) ponderomotive potential is usually approximated by the jitter energy of electrons in the parallel rf field,

$$\Psi \sim \frac{1}{2} m_e \widetilde{u}_\parallel^2 = \frac{e^2 E_\parallel^2}{4 m_e \omega^2} \approx 11 \left(\frac{E_\parallel (V/cm)}{f(MHz)} \right)^2 eV \qquad (3)$$

where the units of the final form are Ψ(eV), E(V/cm) and f(MHz) = $\omega/2\pi$. [Equation (3) is adequate for estimation purposes, but often the contribution to Ψ from $E_\perp$ is also of the same order.] For representative electric fields $E_\parallel \sim 300$ V/cm and frequencies < 100 MHz or so, the condition of strong nonlinear interactions, $\Psi > T$ (e.g. in the SOL or at the separatrix) is easily met in all but the highest frequency experiments. [3] The result of the parallel ponderomotive force $\propto -\nabla_\parallel \Psi$, for adiabatic electrons along the equilibrium magnetic field, is strong expulsion. Additionally, the strong nonlinearity condition $\Psi >$

T typically implies that wave-wave (e.g. parametric) interactions need to be considered, a point which we return to subsequently.

Measurements from the DIII-D tokamak [54] showed that as the power is raised the effect on the *reactive* loading of the antenna is the same as moving the plasma away from the antenna, and is consistent with a ponderomotive expulsion interpretation. Basically, the reactive loading is dominated by the parallel electron current response, and scales with local plasma density in front of the antenna. In this picture, moving the antenna back from the plasma is roughly equivalent to expelling plasma from near the antenna. These experiments suggest that a key difficulty in launching high power IBW is propagating it though the SOL. Due to the ponderomotive expulsion effect, the waves will "dig a channel" in the plasma. At the resulting low local density, the antenna will launch the EPW. The physics is thus rather similar to the problem of ponderomotive effects on lower-hybrid wave propagation, considered e.g. in Ref. 55. A key question becomes whether the EPW can successfully mode transform into the IBW in the presence of this steep channel.

Many large-tokamak IBW experiments have shown that the loading *resistance* is large and insensitive to the frequency (i.e. to the location of cyclotron resonance with respect to the antenna). This feature was not expected from traditional direct launch IBW theory, but could be explained by a linear theory model [56] which assumed ponderomotive depletion of density in front of the antenna, and allowed the energy to be absorbed at the ensuing lower hybrid resonance (LHR) where the EPW to IBW mode transformation would normally occur. A related 1-D nonlinear model, [57] which explicitly included ponderomotive profile steepening, showed enhanced wave reflection

near the LHR that effectively channeled energy into a coaxial mode propagating in the halo plasma. Furthermore, the phasing properties of this mode were consistent with loading and heating efficiency measurements during TFTR IBW direct launch experiments. [58 - 60] The basic idea is that the longer *poloidal* wavelength in 0-0 poloidal phasing enables a shorter radial wavelength parasitic coaxial mode to fit in the halo plasma between the LHR and the wall.

These observations may underlie some of the differences observed between IBW heating in small and large machines, and generally supports the view that ponderomotive effects are responsible through local density profile modification near the antenna. The density expulsion tends to channel the launched wave energy along B into the halo plasma in the form of an EPW or coaxial mode (especially on larger machines where the mode "fits"), rather than radially towards the core plasma in the form of an IBW. Because of the inverse scaling of Ψ in Eq. (3) with wave frequency, it is generally believed that the ponderomotive effects are more deleterious in low frequency experiments, and may be at least partly mitigated by employing high frequency wave-guide launchers [61].

In addition to the strong rf sheaths and ponderomotive effects expected for slow wave launch, parametric decay instability (PDI) is often observed in IBW experiments. [62] An example of probe observations of PDI-generated daughter waves is shown in Fig. 9. While the large field amplitudes present in IBW experiments allow the greatest margin for exceeding parametric decay thresholds, parametric decay has also been observed in FW experiments, and its presence has been invoked to explain an observed edge fast ion population and/or edge ion heating in ASDEX, TEXTOR, JT-60, and

Alcator C-Mod. [63−66] Recently, observations of PDI correlated with edge ion heating have been reported during HHFW heating experiments on NSTX. [67] Parametric decay may be important in deciding what happens to wave energy that is trapped in the edge; however, it has been difficult to measure the power going into the PDI daughter waves.

To describe the parametric decay interaction theoretically, one considers a large amplitude pump wave at frequency and wavenumber (ω_0, $\mathbf{k}_0$), and it is presumed that there are two other modes in the plasma at frequencies and wavenumbers which add up to (ω_0, $\mathbf{k}_0$), called the daughter waves, denoted by (ω, $\mathbf{k}$), (ω_-, $\mathbf{k}_-$). The wave equation for each daughter mode is driven by a nonlinear beat current of the other daughter with the pump,

$$[(c/\omega)^2 \nabla \times \nabla \times \ - \varepsilon \cdot] \ \mathbf{E}(\omega) \propto \mathbf{E}(\omega_0)\mathbf{E}(\omega_-) \tag{4}$$

The initially small daughter waves can be linearly unstable above a certain threshold pump wave amplitude, which typically depends on the damping rates of the daughter modes. This instability is the PDI. In addition to considering two propagating daughter modes, it is also possible to consider a process where one of the daughter modes is replaced by a plasma resonance, or "quasi-mode" such as the $\omega = n\Omega_i$ cyclotron resonance. Often, the wave-number and frequency matching conditions can be met more easily with quasi-mode interactions, e.g. the cyclotron resonance quasi-mode imposes no restriction on $\mathbf{k}_\perp$. Ion cyclotron quasi-mode interactions have been of particular interest with regard to understanding the edge heating and ion tail formation observed in experiments [63-66] because quasi-mode damping provides a mechanism for direct heating of $v_\perp$ by ion cyclotron resonant interaction.

In the so-called dipole approximation (i.e. that of a long wavelength pump), the theoretical analysis can be done linearly by transforming to an oscillating frame, viz. the frame of the jitter in the pump wave field. In this case the *species-dependent* jitter is the underlying physical effect that provides the mode coupling and free energy that make the PDI process unstable. Indeed, PDI thresholds are generally lower in multiple ion species plasmas. [68] The nonlinear coupling coefficient is of order $\mu \sim \mathbf{k} \cdot \mathbf{u}_0 / \omega_0$ where $\mathbf{k}$ is the daughter wavenumber and $\mathbf{u}_0$ is the jitter velocity in the pump wave field. (Thus, $\mathbf{u}_0 / \omega_0$ is the spatial excursion of the jitter motion.) The condition $\mu \sim 1$ provides an initial rough estimate of the wave amplitudes for which parametric processes should be very strong.

In the most common parametric decay processes of interest for both FW and IBW pumps, it turns out that the IBW is one of the daughter modes. [69] Estimating $\mathbf{k} \sim 1/\rho_i$ and $\omega_0 \sim \Omega_i$ one obtains $\mu \sim u_0/v_i$ and $\mu^2 \sim \Psi/T$. Thus strong ponderomotive and parametric interactions may occur simultaneously. Furthermore, for electrostatic modes the wave energy density W_{rf} is roughly $W_{rf} \sim n m u_0^2 \sim n\Psi$. These estimates suggest that the ratio of wave energy density to thermal energy density is an important parameter controlling the virulence of PDI. In specific applications, the actual threshold pump amplitudes for PDI depend on many other considerations. Threshold predictions generally require detailed analysis taking into account the polarization, dispersion and damping properties of the particular modes involved and the implications of the constraints of frequency and wave-number matching.

The linear theory of PDI (i.e. linear in the sense of a fixed pump wave) needed to analyze the threshold conditions systematically is rather well developed for the FW and IBW cases of interest for fusion plasmas. [69] In spatially homogenous problems these

calculations predict the threshold (i.e. marginally stable) electric field amplitude, and above threshold, the temporal growth rate γ (i.e. one obtains absolute instability). When wave propagation through a region of finite spatial extent L is considered, spatial amplification $\sim \exp(\gamma L/v_g)$ results above threshold (convective instability). In inhomogeneous plasmas, the local dispersion relation makes $\mathbf{k} = \mathbf{k(x)}$, and the wavenumber matching conditions can only be maintained over a finite spatial interaction region. This physics sets an effective L.

The tendency for PDI to be stronger (at fixed wave amplitude) in low density, low temperature plasmas, suggests that PDI could be mitigated by launching waves deeper into the edge plasma. The importance of waveguide positioning as a control parameter was considered in an analysis of IBW launch in FTU [61], where it was shown that there are competing constraints on the optimal SOL density: high to reduce PDI, but low to reduce reflected power for good linear coupling. It is also pertinent to note that ponderomotive effects can change the local plasma conditions near a launcher [62] and thus influence PDI thresholds.

In addition to three-wave parametric decay processes, other wave-wave processes can be important when the wave energy density is large. Nonlinear ion-cyclotron (Landau) damping has been shown to efficiently absorb IBW wave energy at half-harmonics of the cyclotron frequency by a mechanism which invokes the nonlinear self-interaction of Bernstein waves. [70] In this case, the nonlinear beating of the IBW with itself can resonate with a quasi-mode, transferring energy to the particles.

Theoretically, fully nonlinear calculations (including pump depletion) of parametric decay and nonlinear Landau damping are very difficult. For IBW, the theory

must include kinetic, hot plasma dynamics, and two or three spatial dimensions for realistic results. This problem presents an opportunity for future theory and simulation.

To summarize this section, a number of nonlinear mechanisms (ponderomotive, parametric and self-interaction) inhibit the efficient propagation of IBW waves into the core plasma and lead to dissipation of the wave energy in the edge region by sheath, collisional, or resonant absorption processes.

4. Slow wave core interactions: flow drive

In many experiments spanning several decades, it was found that directly launched IBW power could trigger improved confinement regimes in a tokamak.[71-77] One example is the use of injected IBW power to produce a core transport barrier in the PBX-M experiment. [74] A steepening of gradients was observed at the region of resonant absorption. Inside this layer, plasma density and temperature increased showing an improved confinement that was named the core-H (CH) mode. This experiment did not measure poloidal flow but observed changes in toroidal flow and its shear near the resonance layer. In other experiments, there were observations of IBW-induced flows. [78, 79], but not necessarily confinement improvement. Collectively, experiments show that the IBW can drive flows, and that the IBW can sometimes enhance confinement, however the mechanisms have not been fully established experimentally.

Plasma turbulence research has shown that sheared flows can suppress turbulence. [80-82] This knowledge has stimulated theoretical work on the calculation of rf driven flows, beginning with the pioneering work of Craddock and Diamond [83] and continuing up to the present. [61,84-91] A number of 1-D and ray tracing calculations

established that local absorption of IBW power at a cyclotron resonance was accompanied by redistribution of momentum that resulted in sheared poloidal (bipolar) flows.

Theoretically and experimentally, the direct launch IBW scheme for flow drive and turbulence suppression appears to be plausible, but practically it can be difficult to get the IBW power into the plasma, as noted in the previous section. This raises the question of whether mode-converted slow waves such as the IBW or ICW could be used to drive flows while avoiding the problems associated with direct IBW launch. A similar approach was proposed earlier for current drive by mode-converted slow waves. [92]

When the FW encounters a mode conversion (MC) layer in a multi-ion-species plasma, both the IBW and the ICW can result as mode conversion products. [90,93,94] New diagnostics, such as phase contrast imaging, have allowed these waves to be observed directly [95] and have helped to stimulate new theoretical work on flow drive, generalizing the previous work to handle MC, hot plasmas, and general electromagnetic waves.

To understand the wave properties required for driving flows, we consider in Figure 10 the three basic mechanisms by which an RF wave can induce forces on a plasma. The first one can be thought of as photon absorption, in which the rf wave energy that is absorbed also imparts a corresponding momentum (proportional to $\mathbf{k}/\omega$) to the plasma. This process is most effective for slow waves, with their relatively large $\mathbf{k}$. Note that this is fundamentally a dissipative force.

The second mechanism can be described as photon reflection. In the extreme case of total reflection, the force is $2\mathbf{k}/\omega$ times the one-way power flow. However, this

mechanism is better thought of in terms of reactive ponderomotive forces, driven by the gradient of the electric field amplitude rather than the circulating power. It is fundamentally non-dissipative.

The third mechanism is a momentum redistribution mechanism related to the Reynolds stress. No net force can be supplied by this mechanism, but adjacent flux surfaces can acquire equal and opposite forces and thereby create sheared flows. The nonlinear stress tensor which describes this process contains both the mechanical Reynolds stress component **vv** and the electromagnetic stress **BB**. For an electromagnetic wave there can sometimes be cancellations between the two pieces. [83, 96, 88]

There are several elegant formalisms for calculating nonlinear plasma effects due to rf waves, including guiding center [97] and quiver kinetics [98] formulations. Recently, flow drive work [86, 91] has been developed using a different formulation, that of the W matrix [99, 100] developed to describe energy flow and absorption in the presence of nonlocality introduced by finite gyroradius effects. This formalism uses a global Fourier representation of the rf fields, and is well suited to implementation in Fourier based codes.[101] The matrix $W(\mathbf{k}, \mathbf{k}')$ is the generalization of the usual hot plasma conductivity matrix $\sigma(\mathbf{k})$ to the nonlocal case. Thus the familiar $\mathbf{J} \cdot \mathbf{E}$ expression for absorbed power is generalized to

$$P_{rf} = \frac{1}{4} \sum_{kk'} e^{i(\mathbf{k'}-\mathbf{k})\cdot\mathbf{r}} \mathbf{E}_k^* \cdot W(\mathbf{k},\mathbf{k}') \cdot \mathbf{E}_{k'} + cc \qquad (5)$$

Analogous to the energy moment of the Vlasov equation from which P_{rf} arises, one can take the momentum moment. In this case the nonlinear driving terms are the forces, which include the Lorentz force and the divergence of a nonlinear stress tensor

which involves the second order distribution function. It is shown in Ref. 91 that the total force on a fluid element can be expressed in terms of the three basic mechanisms, direct absorption, reactive ponderomotive force, and momentum redistribution. The reactive ponderomotive term reduces exactly to well known expressions in the fluid limit. Furthermore, flux-surface-averaged plasma flows in a tokamak can be driven only by the dissipative forces. Remarkably, these may be expressed simply in terms of the W matrix.

$$\mathbf{F}_{dis} = \mathbf{F}_{abs} + \mathbf{b} \times \nabla X_d \tag{6}$$

$$\mathbf{F}_{abs} \approx \frac{1}{4\omega}(\mathbf{k} + \mathbf{k}')\mathbf{E}_k^* \cdot W(\mathbf{k},\mathbf{k}') \cdot \mathbf{E}_{k'} + \text{c.c.} \sim \frac{\mathbf{k}}{\omega} P_{rf} \tag{7}$$

$$X_d \approx \frac{P_\perp}{2\Omega} \sim \frac{n}{2\omega}\mathbf{E}_k^* \cdot W_n(\mathbf{k},\mathbf{k}') \cdot \mathbf{E}_{k'} \tag{8}$$

The direct absorption term $\mathbf{F}_{abs}$ can drive net flows, depends on the momentum in the waves, and is effective with either electron or ion dissipation. The dissipative stress (momentum redistribution) term $\mathbf{b} \times \nabla X_d$ drives bipolar sheared flows but no net flows. It depends on the power absorbed in the perpendicular direction [91] and scales inversely with the cyclotron frequency [or, in the second form of Eq. (8), is proportional to the gyro-harmonic number n], so the dissipative stress term is only significant for ions. In general, flow drive is largest for short wavelengths and narrow dissipation layers, the narrow layers implying stronger shear in the flow.

This flow drive theory was implemented in the AORSA code [90] and applied to a C-Mod mode-conversion case which generates both IBW and ICW products, as shown in Fig. 11. The toroidal flow can be obtained by balancing the rf force with an empirical diffusion of toroidal angular momentum. For 1 MW of power, the flow is in the range of a few km/s and the peak shearing rate is about 10^4 s^{-1}, which is somewhat small for

effective turbulent suppression. To date, a careful survey of parameter space for more optimal cases has not been done. Also, there are some subtleties in converting forces to flows, that bring in both neoclassical and turbulent transport theory. More theoretical work is needed in this area, particularly including time transients and anomalous diffusion which couple the poloidal and toroidal flows in the theory. Experiments that exhibit rf-induced confinement improvement and have the diagnostic capability to make measurements of poloidal and toroidal velocity shear are also needed, as well as experimental validation of flows from mode-converted waves.

Turbulence suppression is approximately governed by the shear in the radial electric field. There are different mechanisms for modifying E_r shear by applied rf waves that can be seen from the steady state ion radial force balance equation.

$$\frac{v_\zeta B_\theta - v_\theta B_\zeta}{RB_\theta} \equiv G(\psi) = -c\left(\frac{\partial \Phi}{\partial \psi} + \frac{1}{Zen_i}\frac{\partial p_i}{\partial \psi}\right) + \left\langle \frac{c}{Zen_i}\frac{F_{i\psi}}{RB_\theta}\right\rangle_\psi \qquad (9)$$

The flux function $G(\psi)$, representing the $\mathbf{v}\times\mathbf{B}$ flow term, balances the radial electric field, the ion pressure gradient and any external radial forces. Nonlinear wave momentum processes (poloidal and toroidal forces) drive corresponding flows, as discussed in the preceding paragraphs; rf heating can modify the ion pressure profile locally, changing ∇p_i; and finally, in principle, the waves can exert a direct *radial* ponderomotive force, although in practice this is almost always negligible in large tokamaks.

Like the other volume nonlinear effects (e.g. ponderomotive and parametric), the forces available for flow drive are proportional to wave amplitude squared, or wave energy density. However, to drive flows in the poloidal or toroidal direction, the wave forces must only compete with the relatively weak friction forces and or radial diffusion

provided by neoclassical and turbulent processes. Thus, in principle, significant rf-driven sheared flows are possible in situations where the wave energy density is very small compared with the thermal energy density.

While existing theoretical modeling and experimental work show that it is difficult to create rf-induced transport barriers in large tokamaks, further work in this area is warranted by the rather exciting potential payoff: the promise of being able to create and control transport barriers on demand, both in location and strength. In addition to the obvious applications for practical performance and control of fusion plasmas, the ability to drive sheared flow layers would allow many interesting physics experiments to illuminate nonlinear turbulent transport physics and tokamak profile evolution.

5. Integrated modeling: the new forefront

The issues discussed in the preceding sections have important implications for integrated modeling, which is an exciting new forefront in rf physics. Integrated modeling can play an important role in hardware design, scenario development (including not only core rf physics, but now also nonlinear edge rf physics) and in the interpretation of experimental results.

One promising area is the incorporation of more edge physics into antenna coupling codes, such as plasma in the antenna region, rf interaction with blobs and turbulence (self-consistent density at the antenna for coupling, wave scattering from blobs and fluctuations, and effect of rf-driven flows on the turbulence), sheath and ponderomotive effects and surface physics (e.g. sputtering, neutral gas desorption, and arcing).

Inclusion of this physics would provide a predictive capability for plasma loading with a self-consistent density profile. At present, there is no robust way of predicting in advance the antenna loading for future experiments, mainly because the edge and SOL density profile is not known. Additionally, this type of integrated modeling could predict some operational constraints on the antenna due to problems such as local power dissipation, hot spot damage, and possibly certain types of arcs. An ambitious goal would be a completely self-consistent description of the effects of rf on the edge (e.g. turbulence), and vice versa. Some work in this direction is in progress [20, 22, 32]

For such a computational project to succeed, validation of codes with experiments at the most fundamental level is necessary. Low power loading measurements [41] would provide a very useful tool in this regard, as well as yielding a direct experimental diagnosis of sheaths, local plasma density, and antenna-plasma interactions [16].

A second promising area for integrated modeling is that of more realistic edge conditions for global full-wave rf codes. Typically in these codes, all the launched power is absorbed in the core no matter how weak the core absorption is. It is known from experiments that edge physics (and the resulting "anomalous" absorption of wave energy) is especially important for cases in which the spectrum is dominated by low $k_\parallel$ modes. More realistic models of edge dissipation are needed, for example employing boundary conditions to model sheaths. [19-22] Edge collisions and neutrals may also be important in some cases. Incorporation of the missing edge physics will allow a new predictive capability for lost power and heating efficiency.

6. Conclusions

In conclusion, nonlinear effects are generally important for ICRF waves at the edge and can also be important in the core for short-wavelength, slow waves such as the IBW and ICW. Many important individual pieces of nonlinear RF interactions are at least partially understood as isolated phenomena. These include rf-sheaths (and their role on impurities, power dissipation, hot spots, convection, and SOL currents), ponderomotive effects, far field sheaths and edge dissipation, parametric decay, nonlinear self-interaction, and rf effects on plasma flows and E_r.

It is highly desirable to bring these individual pieces together in a way that can be useful for improved understanding of existing experiments, for extrapolation into new regimes, and for reliable scenario development on large tokamaks and future burning plasma experiments. Some pieces of the required integration have been accomplished conceptually in specialized models, but it is likely that large scale integration of these phenomena in rf-edge modeling computer codes will be necessary to achieve a predictive capability for rf-edge interaction that has so far been elusive. It is well established that deleterious nonlinear edge interactions can determine the outcome of experiments, limiting the parameter space available for successful operation. [A notable example is the restricted use on many experiments of non-dipole (low-$k_\parallel$) phasing because of low coupling efficiency, due to the nonlinear processes discussed in Sec. 2.] The core physics of rf wave propagation and absorption are relatively well understood and experimentally validated; a similarly validated predictive model for nonlinear edge interaction presents a challenging but extremely worthwhile goal for the ICRF theory and simulation community.

Recent progress towards a long-pulse burning plasma experiment provides strong motivation in this direction. With the ever increasing availability of large scale computing resources, and continued developments in the software infrastructure required for such projects, there is hope that the goal of reliable predictive rf-edge interaction codes will prove to be feasible. Efforts in this direction are warranted for advancing the utility of ICRF waves in heating, current drive and novel applications for future fusion and burning plasma experiments.

Acknowledgments

References

1.   Noterdaeme J.-M, 1992 AIP Conf. Proc. **244** 71.

2.   Noterdaeme J.-M. and Van Oost G. 1993 Plasma Phys. Control. Fusion **35** 1481.

3.   Ono M. 1993 Phys. Fluids B **5** 241.

4 .   Myra J. R., D'Ippolito D. A., Russell D. A., Berry L. A., Jaeger E. F. and Carter M. D., 2005 AIP Conf. Proc. **787** 3.

5.   Jaeger E. F., Harvey R. W., Berry L. A., Myra J. R. *et al* 2006, Nucl. Fusion (this issue).

6.   Adam J. 1987 Plasma Phys. Control. Fusion **29** 443.

7.   Bures M., Jacquinot J., Lawson K., Stamp M., *et al* 1991 Plasma Phys. Control. Fusion **33** 937.

8.   Bures M., Jacquinot J. J., Stamp M. F. *et al* 1992 Nucl. Fusion **32** 1139.

9.   Bures M., Bhatnagar V. P., Jacquinot J., Morgan P. and Start D. F. H. 1988 Plasma Phys. Control. Fusion **30** 1833.

10.   Butler H. S. and Kino G. S. Phys. 1963 Fluids **6** 1346.

11.   Perkins F. W. 1989 Nucl. Fusion **29** 583.

12.   Chodura R. and Neuhauser J. 1989 16th Eur. Conf. on Contr. Fus. Plasma Phys., Venice, Vol. III, p. 1089.

13.   Brambilla M., Chodura R., Hoffmann J. *et al*, in *Plasma Physics and Controlled Nuclear Fusion Research 1990* (Proc. 13th Int. Conf. Washington DC, 1990) Vol. 1, p. 723, IAEA, Vienna (1991).

14.   Van Nieuwenhove R. and Van Oost G. 1989 J. Nucl. Mater. **162-164** 288.

15. Myra J. R., D'Ippolito D. A. and Gerver M. J. 1990 Nuclear Fusion **30** 845.

16. D'Ippolito D. A. and Myra J. R. 1996 Phys. Plasmas **3** 420.

17. Greene G. J., *ICRF Antenna Coupling and Wave Propagation in the Caltech Research Tokamak*, Ph. D. dissertation, California Institute of Technology, Pasedena, CA (1984).

18. Lieberman M. A. 1988 IEEE Trans. Plasma Sci. **PS-16** 638.

19. Jaeger E. F., Berry L. A., Tolliver J. S. and Batchelor D. B. 1995 Phys. Plasmas **2** 2597.

20. Carter M. D., D'Ippolito D. A., Myra J. R. and Russell D. A. 2005 AIP Conf. Proc. **787** 218.

21. Myra J. R., D'Ippolito D. A. and Bures M. 1994 Phys. Plasmas **1** 2890.

22. D'Ippolito D. A., Myra J. R., Russell D. A. and Carter M. D. 2005 AIP Conf. Proc. **787** 222.

23. Wukitch. S. J., Boivin R. L., Bonoli P. T. *et al* 2004 Plasma Phys. Control. Fusion **46** 1479.

24. D'Ippolito D. A., Myra J. R., Bures M. and Jacquinot J. 1991 Plasma Phys. Cont. Fusion **33** 607.

25 . Colas L., Heuraux S., Bremond S. and Bosia G. 2005 Nucl. Fusion **45** 767.

26. Myra J. R., D'Ippolito D. A. and Ho Y. L. 1996 Fusion Eng. Design **31** 291.

27. Swain D. W. *et al* 2003 Fusion Sci. Tech. **43** 503.

28. D'Ippolito D. A., Myra J. R., Jacquinot J. and Bures M. 1993 Phys. Fluids B **5** 3603.

29. Moyer R. A., Van Niewenhove R., Van Oost G. *et al* 1991 J. Nucl. Mater **176-177** 293.

30. Diebold D. A., Majeski R., Tanaka T. *et al* 1992 Nucl. Fusion **32** 2040.

31. Colas L., Costanzo L., Desgranges C. *et al* 2003 Nucl. Fusion **43** 1.

32. Colas L., Faudot E., Brémond S., Heuraux S. 2005 AIP Conf. Proc. **787** 150.

33. Bécoulet M., Colas L., Pécoul S. *et al* 2002 Phys. Plasmas **9** 2619.

34. Faudot E., Heuraux S. and Colas L. 2005 AIP Conf. Proc. **787** 214.

35. Jaeger E. F., Carter M. D., Berry L. A., Batchelor D. B. *et al* 1998 Nucl. Fusion **38** 1.

36. Lieberman M. A. and Godyak V. A. 1998 IEEE Trans. Plasma Sciences **26** 955.

37. D'Ippolito D. A., Myra J. R., Rogers J. H., Hill K. W. *et al* 1998 Nucl. Fusion **38** 1543.

38. Krasheninnikov S. I. 2001 Phys. Lett. A **283** 368.

39. D'Ippolito D. A., Myra J. R. and Krasheninnikov S. I. 2002 Phys. Plasmas **9** 222.

40. Russell D. A., D'Ippolito D. A. and Myra J. R. 2004 Bull. Amer. Phys. Soc. **49** 84 (paper CP1.066).

41. Swain D. W., Pinsker R. I., Baity F. W., Carter M. D. *et al* 1997 Nucl. Fusion **37** 211.

42. Majeski R., Probert P. H., Tanaka T., Diebold D. *et al* 1994 Fusion Eng. Design **24** 159.

43. Sorensen J., Diebold D. A., Majeski R., Hershkowitz N. 1996 Nucl. Fusion **36** 173.

44. Myra J. R., D'Ippolito D. A., Rice J. A. and Hazelton C. S. 1997 J. Nucl. Mater **249** 190.

45. D'Ippolito D. A., Myra J. R., Rice J. A. and Hazelton C. S. 1997 AIP Conf. Proc. **403** 463.

46. Van Nieuwenhove R. and Van Oost G. 1992 Plasma Phys. Control. Fusion **34** 525.

47. D'Ippolito D. A., Myra J. R., Ryan P. M., Righi E. *et al* 2002 Nucl. Fusion **42** 1357.

48. Bohdansky J. 1984 in *Data Compendium for Plasma-Surface Interactions, Nucl. Fusion Special Issue*, p. 61; and corrections in 1984 Nucl. Fusion **24** 1683.

49. Perkins F. W. 1989 Bull. Am. Phys. Soc. **34** 2093 (paper 6S6).

50. Myra J. R. and D'Ippolito D. A. 1994 Phys. Plasmas **1** 2890.

51. McCarthy A. L., Bhatnagar V., Bures M. *et al* 1988 in *Control. Fusion and Plasma Heating* (Proc. 15th Eur. Conf. Dubrovnik), Vol 12B, Part II, European Physical Society p. 717.

52. Hellsten T. and Laxåback M. 2005 Phys. Plasmas **12** 032505.

53. Cesario R., De Marco F., Cardinali, A. and Brambilla M., 1994 Nucl. Fusion **34** 1527.

54. Mayberry M. J., Pinsker R. I., Petty C. C., Porkolab M. *et al* 1993 Nucl. Fusion **33** 627.

55. Morales G.J., 1977 Phys. Fluids **20** 1164.

56. Chiu S. C., Mayberry M. J., Pinsker R. I., Petty C. C., Porkolab M. 1992 AIP Conf. Proc. **244** 169.

57. Russell D. A., Myra J. R. and D'Ippolito D. A. 1998 Phys. Plasmas **5** 743.

58. Wilson J. R., Bell R. E., Bernabei S. *et al* 1998 Phys. Plasmas **5** 1721.

59. Myra J. R., D'Ippolito D. A., Russell D. A., Rogers J. H., Intrator T. 2000 Phys. Plasmas **7** 283.

60. Intrator T., Myra J. R. and D'Ippolito D. A., 2003 Nucl. Fusion **43** 531.

61. Cardinali A., Castaldo C., Cesario R. *et al* 2002 Nucl. Fusion **42** 427.

62. Pinsker R. I., Petty C. C., Mayberry M. J., Porkolab M. *et al* 1993 Nucl. Fusion **33** 777.

63. Van Nieuwenhove R., Van Oost G., Noterdaeme J.-M., Brambilla M., Gernhardt J. and Porkolab M. 1988 Nucl. Fusion **28** 1603.

64. Van Oost G., Van Nieuwenhove R., Koch R., Messiaen A. M. *et al* 1990 Fusion Eng. Design **12** 149.

65. Fujii T., Saigusa M., Kimura H., Ono M. *et al* 1990 Fusion Eng. Design **12** 139.

66. Rost J. C., Porkolab M. and Boivin R.L. 2002 Phys. Plasmas **9** 1262.

67. Wilson J. R. *et al* 2005 AIP Conf. Proc. **787** 66.

68. Sperling J. L. and Perkins F. W.1974 Phys. Fluids **17** 1857.

69. Porkolab M. 1990 Fusion Eng. Design **12** 93.

70. Porkolab M. 1985 Phys. Rev. Lett. **54** 434.

71. Ono M., Beiersdorfer P., Bell R., Bernabei S. *et al* 1988 Phys. Rev. Lett. **60** 294.

72. Seki T., Kawahata K., Ono M., Ida K. *et al* 1991 AIP Conf. Proc. **244** 138.

73. Moody J. D., Porkolab M., Fiore C. L., McDermott F. S. *et al* 1988 Phys. Rev. Lett. **60** 298.

74. LeBlanc B., Batha S., Bell R., Bernabei S. *et al* 1995 Phys. Plasmas **2** 741.

75. Phillips C. K., Bell M. G., Bell R. E., Bernabei S. *et al* 2000 Nucl. Fusion **40** 461.

76. Cesario R., Cardinali A., Castaldo C., Leigheb M. *et al* 2001 Phys. Plasmas **8** 4721.

77. Wan B, Zhao Y., Li J. *et al* 2003 Phys. Plasmas **10** 3703.

78. LeBlanc B. P., Bell R. E., Bernabei S., Hosea J. C. *et al* 1999 Phys. Rev. Lett. **82** 331.

79. Riccardi C., Colle F. De, Fontanesi M., Petty C. C. *et al* 2001 AIP Conf. Proc. **595** 83.

80. Biglari H., Diamond P. H. and Terry P. W. 1990 Phys. Fluids B **2** 1.

81. Burrell K. H., Carlstrom T. N., Doyle E. J. *et al* 1992 Plasma Phys. Control. Fusion **34** 1859.

82. Terry P. W. 2000 Rev. Mod. Phys. **72** 109.

83. Craddock G. G. and Diamond P. H. 1991 Phys. Rev. Lett. **67** 1535.

84. Ono M. *et al* 1995 in *Plasma Phys. Control. Nucl. Fusion Res. 1994* (Proc. 15th Int. Conf. Seville, 1994), Vol. 1, p. 469, IAEA, Vienna (1995).

85. Berry L. A., Jaeger E. F. and Batchelor D. B. 1999 Phys. Rev. Lett. **82** 1871.

86. Jaeger E. F., Berry L. A. and Batchelor D. B. 2000 Phys. Plasmas **7** 3319.

87. Elfimov A. G., Amarante-Segundo G. *et al* 2000 Phys. Rev. Lett. **84** 1200.

88. Myra J. R. and D'Ippolito D. A. 2000 Phys. Plasmas **7** 3600.

89. Weitzner H., Berry L. A., Jaeger E. F. and Batchelor D. B. 2000 Phys. Plasmas **7** 564.

90. Jaeger E. F., Berry L. A., Myra J. R., Batchelor D. B. *et al* 2003 Phys. Rev. Lett. **90**, 195001.

91. Myra J. R., Berry L. A., D'Ippolito D. A. and Jaeger E. F. 2004 Phys. Plasmas **11** 1786.

92. Majeski R., Phillips C.K. and Wilson J.R. 1994 Phys. Rev. Lett. **73** 2204.

93. Perkins F. W. 1977 Nucl. Fusion **17** 1197.

94.   Nelson-Melby E. *et al* 2003 Phys. Rev. Lett. **90** 155004.

95.   Lin Y., Wukitch S., Parisot A., Wright J. C. *et al* 2005 Plasma Phys. Control. Fusion **47** 1207.

96.   Kim E. J., Hahm T. S. and Diamond P. H. 2001 Phys. Plasmas **8** 3576.

97.   Cary J. R. and Kaufman A. N. 1981 Phys. Fluids **24** 1238.

98.   Catto P. J. *et al* 1990 Phys. Fluids B **2** 2395.

99.   Smithe D. N. 1989 Plasma Phys. Control. Fusion **31** 1105.

100. Brambilla M. 1998 *Kinetic Theory of Plasma Waves* (Clarendon Press, Oxford).

101. Jaeger E. F., Berry L. A., D'Azevedo E. D. *et al* 2001 Phys. Plasmas **8** 1573.

Figure Captions

1. Basic sheath physics. The sheath forms to equalize electron and ion loss rates. The resulting potential enhances electron confinement by forming a potential barrier for electrons, i.e. the sheath of width Δ. The same potential accelerates ions into the plates and causes the dissipation of sheath power. For the rf-sheath, the driving voltages $\pm V_0$ at each end oscillate in time, and the central potential must remain ($\sim 3\ T_e$) above the maximum voltage at either end.

2. Phasing and field-line angle dependence of sheath driving voltages on the front face of a Faraday screen. Sheaths form at the points where the field lines contact the conductor. Large sheath voltages arise in non-symmetric phasings (e.g. monopole) and for large angles between the field line and the Faraday screen. In monopole phasing, the sheath voltage is essentially the fraction of the end-to-end voltage along the current strap that is subtended by the contacts, as indicated by the arrows at left. (adapted from Fig. 3 of Ref. 24)

3. Spatial dependence of sheath-induced potentials. Shown is a small section of the Faraday screen for a mock-up of the TFTR Bay-M antenna. The screen bars are solid grey, gaps are black, and field lines are color coded by sheath voltage. Contact points differ for many closely spaced field lines, causing them to acquire different sheath voltages. The spatial variation of the sheath potential gives rise to **E**×**B** convection. (reprinted from Ref. 26, with permission from Elsevier)

4. IR camera image of the antenna on Tore Supra after 15 s operation at 8 MW ICRF power. (There is no LH power at the time of the picture.) Clearly visible

in the image are hot spots on the antenna front face, especially at the corners, due to the additional heat load driven by RF sheaths. The large hot spot on the main lower part of the limiter at left is the non-rf-specific thermal flux from the SOL. (courtesy of L. Colas and the Tore Supra Group)

5.   Reflectometry-measured radial density profiles (solid lines) near the TFTR antenna, showing ICRF-induced modifications. The positions of the RF limiter surface (x_{RF}) and Faraday screen (x_{FS}) are indicated. During the RF phase, the density is depleted by rf-enhanced convection which "pumps out" plasma. The dashed lines are a fit to a convective-cell model. (reprinted from Ref. 37)

6.   (a) Radial propagation of blobs and interaction with antenna near-field sheaths. The three top panels show the plasma density from a 2D (radial-poloidal) numerical simulation using the SOLT turbulence code for three different times (normalized to Ω_i). Here, a single blob is initialized at t = 0 and convects outward towards the antenna, encountering a spatially-varying antenna sheath potential (convective cell pattern), which distorts the blob and alters its trajectory. The radial positions of the reference surfaces (which determine the parallel connection length to material surfaces) are indicated in the figure: plasma limiter (PL), bumper tile (BT) and Faraday screen (FS). In experiments, the self-consistent density profile near the antenna has a significant contribution from turbulence-generated blobs, modified by antenna-sheath interactions such as those depicted here. (b) Time history of the peak density of the blob. Here the sheath voltage is quite modest: $V_{rf}(FS)/T_e = 4$.

7. Experimental measurement of low power nonlinear loading from the DIII-D fast-wave antenna [41]. The data are consistent with a sheath model [16] that competes the linear dependence of sheath-power dissipation on voltage V, with the standard V^2 dependence of the outgoing Poynting power flux. Comparison of such models with experimental measurements may be useful for diagnosis of sheath effects, for code validation and for model verification. (reprinted from Ref. 41)

8. Generation of an evanescent slow wave and concomitant $E_\parallel$ by a pure fast wave incident on an irregular boundary. Shown are the contours of $E_\parallel$. Here, the background magnetic field $\mathbf{B}_0$ is oriented at 60° to the plane of the page. In general, the standard conducting-wall boundary conditions cannot be satisfied at an irregular material surface without including both fast and slow wave polarizations. The "bump" in the conducting surface at left gives rise to a local rf $E_\parallel$ which can dissipate power through sheaths or collisional mechanisms. In general this mechanism occurs at edge walls and limiters whenever the flux surfaces and conducting boundaries are not coincident. (adapted from Ref. 50)

9. RF probe spectra from DIII-D at two different gain settings. The highest gain setting (lower panel) shows the presence of other modes in addition to the launched mode at 36 MHz, and are evidence for the process of parametric decay instability. PDI activity is correlated with edge ion heating; however, it is difficult to deduce net power lost to the PDI channel from probe data. It was shown that other nonlinear processes, in particular ponderomotive expulsion,

play an important role in describing these experiments [54, 56]   (reprinted from Ref. 62)

10. Three mechanisms for rf-wave induced forces on a plasma: (a) Photon absorption results in a dissipative transfer of momentum $\mathbf{k}/\omega$ for each unit of wave energy absorbed. (b) Photon reflection is non-dissipative and transfers $2\mathbf{k}/\omega$ for each unit of wave energy reflected. This mechanism is equivalent to the reactive ponderomotive force when the description is cast in terms of standing-wave electric field rather than circulating power. (c) Momentum redistribution occurs by the Reynolds stress mechanism in which eddies (e.g. from a propagating wave) transfer canonical momentum p_y in the x direction. Several conditions must be met for non-vanishing flow drive from the Reynolds stress, including phase relationships between oscillating u_x and p_y such that their average does not vanish (e.g. typically from dissipation at a resonance layer) and radial gradients in the wave amplitude. Furthermore, for an electromagnetic wave the mechanical ($\mathbf{vv}$) and electromagnetic ($\mathbf{BB}$) components of the stress can cancel.

11. Simulation of sheared flows with AORSA. Shown here is an Alcator C-Mod case in which a launched fast wave is mode converted to a left-going IBW and a right-going ICW. The ICW propagates into resonance where it is absorbed. The upper panel shows $\mathrm{Re}(E_\perp)$. The lower panel shows the resulting flux-surface-averaged toroidal flows. The calculation is based on steady state toroidal force balance with an empirical toroidal momentum diffusion. (upper panel adapted from Ref. 90)

λ_{de}

$\Phi \approx V_0 + 3T_e$

Δ

$+V_0$
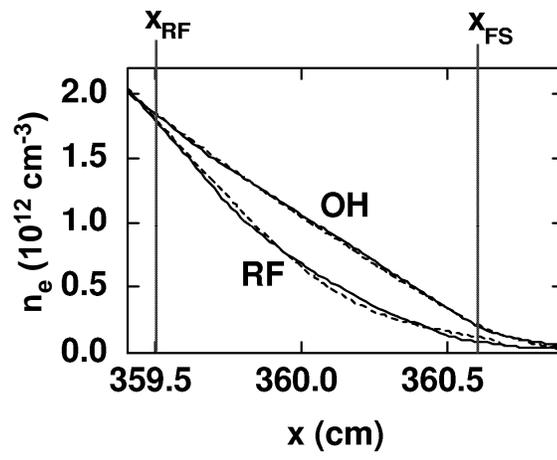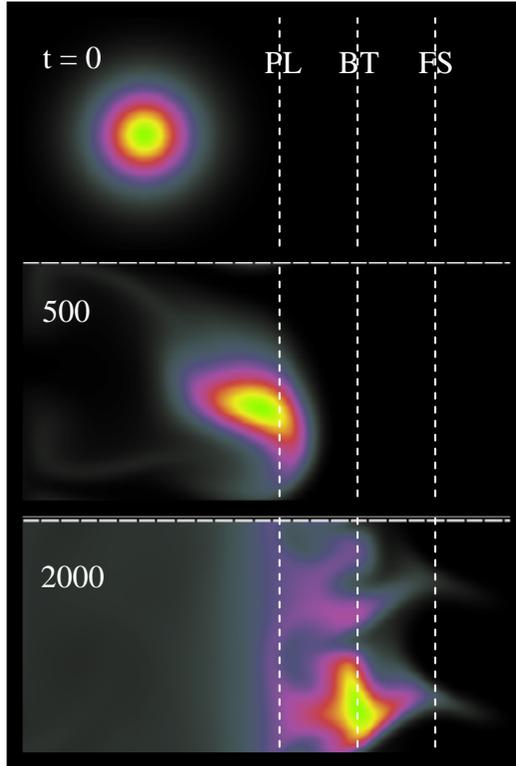
$-V_0$
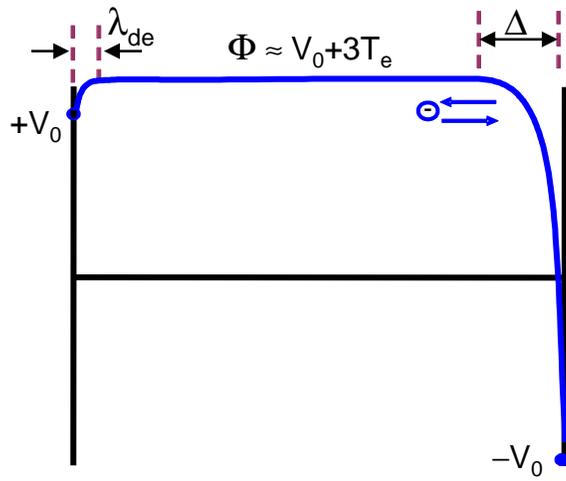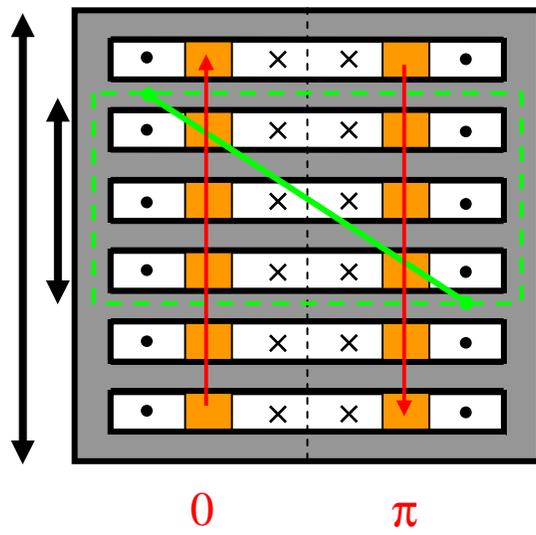
Fig. 1

Fig. 2
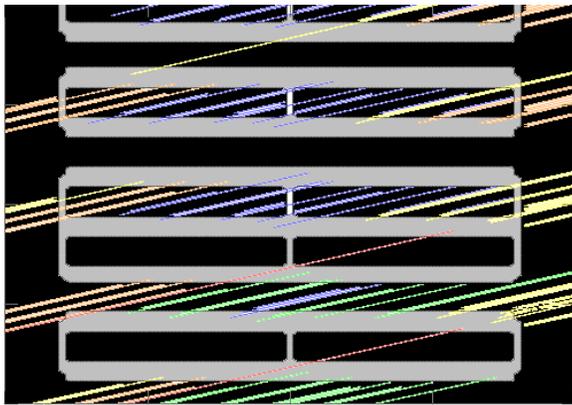
Fig. 3
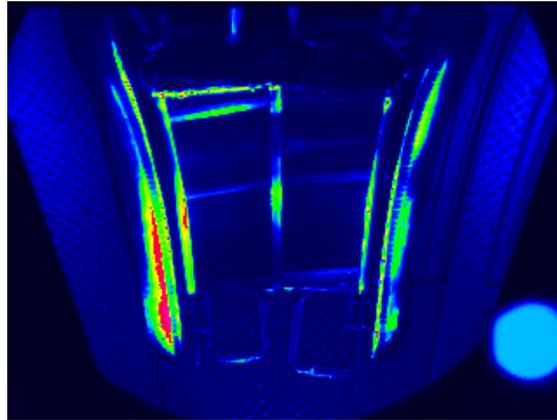
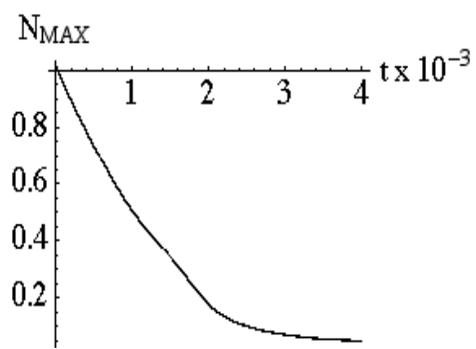color online version
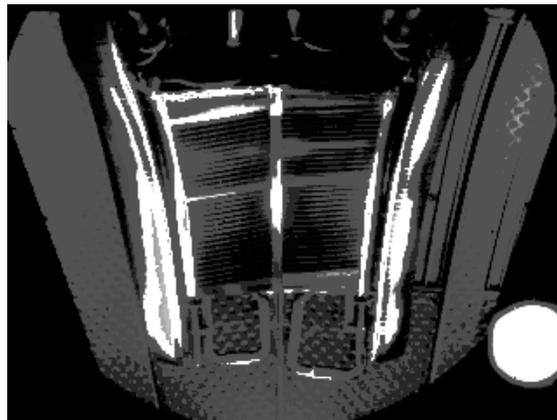
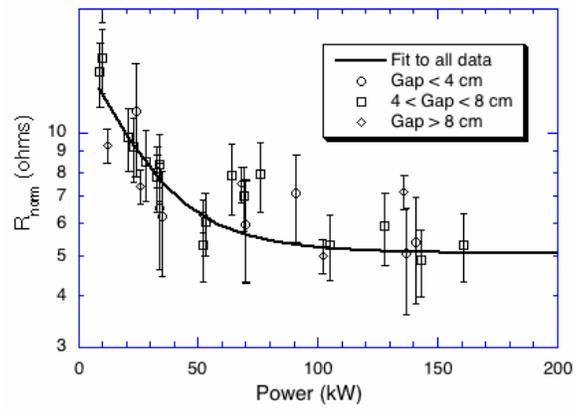B&W print version

Fig. 4

Fig. 5

a)

b)

Fig. 6

Fig. 7
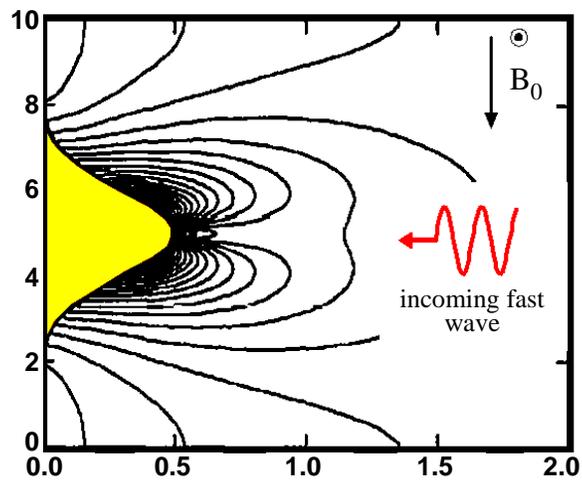
Fig. 8

Fig. 9

a) photon absorption

$\mathbf{k},\ \omega$

b) photon reflection

$\mathbf{k},\ \omega$

c) Reynolds stress

p_y

u_x

Fig. 10

Fig. 11